Experimental Thermal and Fluid Science 124 (2021) 110368

Contents lists available at ScienceDirect

Experimental Thermal and Fluid Science

journal homepage: www.elsevier.com/locate/etfs

On the width and mean value of bubble size distributions under subcooled flow boiling

Marcos Conde-Fontenla [a], Concepción Paz [a,*], Miguel Concheiro [a], Gherhardt Ribatski [b]

[a] CINTECX, Universidade de Vigo, Campus Universitario Lagoas-Marcosende, 36310 Vigo, Spain
[b] Heat Transfer Research Group, Escola de Engenharia de São Carlos, University of São Paulo, Avenida Trabalhador São-Carlense, 400, São Carlos, SP, Brazil

ARTICLE INFO

Keywords:
Subcooled flow boiling
Bubble diameter
Probability distribution function
Width
Mean value
Experimental correlation

ABSTRACT

In this work, a new comprehensive dataset about bubble sizes in flow boiling of water is presented. The experimental setup basically consists of a lower copper heated plate embedded in a horizontal rectangular channel flow. Several experimental conditions, ranging bulk velocities: 0.1–0.9 [$m{\cdot}s^{-1}$]; mass fluxes: 96.9–871.8 [$kg{\cdot}m^{-2}{\cdot}s^{-1}$]; subcooling degrees: 16–36 [°C]; heat fluxes: 200–650 [$kW{\cdot}m^{-2}$] and pressures: 110–190 [kPa] were set for three cooper plates of different roughness, with S_a: 0.45, 1.23 and 7.43 [μm], respectively. Based on the current samples, the probability function for the normalized bubble diameter has been described by a lognormal pdf for any plate and experimental condition and a dimensionless correlation for the standard deviation of the bubble size distribution is presented. In order to completely describe the diameter distribution for bubbles in subcooled boiling systems, an improved correlation for the mean bubble diameter value is also presented here, after a deep review of previously published datasets. Further work is required to accommodate different channel configurations and surface morphologies.

1. Introduction

Determination of bubble size still represents a challenge in the characterization of flow boiling. Several authors in the past has proposed models, both based in an energy balance and force balance. Formally, with the appropriate set of equations, the bubble growing process and the ulterior trajectory can be mathematically described. Nevertheless, the success of energy based and force balance models when being evaluated with other data than own model's data, is relative. A possible explanation of this can be expressed with two factors. On the one hand, the physical mechanisms themselves, since three phase systems are very complex and several scales, both spatial and temporal, do take place. On the other, many of past studies were validated with restricted data both by means of sample size and limited experimental equipment or even they are purely derived from theoretical equations. The problem with the latter it is not the formulation of the model itself, even formulated under acceptable assumptions. The major difficulty is the characterization of the actual magnitude for the properties and the geometries involved. As an example, surface tension force, aerodynamic forces on a bubble or the bubble growth force can be accurately described, but the knowledge of the proper distribution for the contact angle along all the separation line or the shape and pressure center of the bubble actually poses a big problem. In fact, modelling of wall heat flux in heat transfer problems concerning boiling and condensation process, make use of the so-called heat flux partitioning models. This type of models, widely used in CFD solvers, split the total wall heat flux into the individual contributions, such as the pure one phase convection and the boiling heat flux. The calculation of each contribution is usually based on empirical correlations. Even if the aim is to formulate the mechanistic model, solving the physics of the problem by means of momentum and energy equations and no matter the complexity of the equation set is, it is still necessary to have information about the nucleation site density, the bubble release frequency and the bubble size. At the present time, reliable information of such parameters is only available using empirical correlations.

Concerning the previously mentioned correlations, several expressions for the bubble size, releasing frequencies and nucleation site density are available in technical literature, and most of them return a mean value. In some cases, this value is not representative yielding to large errors when employed out the range for what the correlation was developed or simply due to the small size of the sample in which the correlation is based on. Moreover, even when the returned mean value agrees with the entire population, there are many models incorporating

* Corresponding author.
E-mail address: cpaz@uvigo.es (C. Paz).

https://doi.org/10.1016/j.expthermflusci.2021.110368
Received 11 October 2020; Received in revised form 26 January 2021; Accepted 30 January 2021
Available online 6 February 2021

Nomenclature

Bo	Boiling number [–]
c_p	specific (mass) isobaric heat capacity [J/kg/K]
$\widehat{D}$	normalized bubble diameter [–]
D^+	dimensionless bubble diameter $\left(\frac{D_b}{l_c}\right)$ [–]
D_b	bubble diameter [m]
D_{hyd}	hydraulic diameter [m]
Eo	Eötvös number [–]
ΔT_{sub}	subcooling degree $(T_{sat} - T_b)$ [K]
ΔT_w	superheating degree $(T_w - T_{sat})$ [K]
G	mass flux [kg/s/m^2]
g	gravitational acceleration [m/s^2]
h	enthalpy of vaporization [J/kg]
Ja_w	wall Jakob number $\left[\frac{c_{p,L}(T_w - T_{sat})}{h_{LV}}\right]$ [–]
Ja_{sat}	saturation Jakob number $\left(\frac{c_{p,L}T_{sat}}{h_{LV}}\right)$ [–]
Ja_{sub}	subcooled Jakob number $\left[\frac{c_{p,L}(T_{sat} - T_b)}{h_{LV}}\right]$ [–]
Ja_T	total Jakob number $\left[\frac{c_{p,L}(T_w - T_b)}{h_{LV}}\right]$ [–]
k	thermal conductivity [W/K/m]
l_c	capillary length $\left(\sqrt{\frac{\gamma}{g(\rho_L - \rho_V)}}\right)$ [m]
p	pressure [Pa]
Pr	Prandtl number [–]
q	heat flux [W/m^2]
R^2	coefficient of determination [–]
R_a	arithmetical mean height (2D) [m]
Re	Reynolds number [–]
S_a	arithmetical mean height (3D) [m]
S_{AR}	area ratio [–]
S_{dr}	developed interfacial area ratio [–]
T	temperature [K]
T_{1x}	top thermocouple reading [K]
T_{2x}	bottom thermocouple reading [K]
T_Δ	temperature difference $(T_{1x} - T_{2x})$ [K]
T^*	dimensionless temp. diff. $\left(\frac{T_w - T_b}{T_w - T_{sat}}\right)$ [–]
v_b	bulk velocity $\left(\frac{\dot{m}}{\rho_L A}\right)$ [m/s]
x_w	top thermocouple – wall distance [mm]
x_Δ	thermocouple spacing [mm]

Greek

α	thermal diffusivity [m^2/s]
γ	surface tension [N/m]
θ	contact angle [–]
λ	shape parameter n/d
μ	mean value, first parameter n/d
ν	momentum diffusivity [m^2/s]
ξ	error var.
ρ	mass density [kg/m^3]
ρ^*	density ratio $\left(\frac{\rho_V}{\rho_L}\right)$ [–]
σ	standard deviation, second parameter n/d

Subscripts

b	bulk conditions, bubble
exp	experimental
L	liquid
LV	liquid-to-vapor
$pred$	predicted
sat	saturation state
sub	subcooled
sup	superheated
V	vapor
w	wall conditions

Abbreviation

CDF	cumulative distribution function
CFD	computer fluid dynamics
CV	coefficient of variation
EDM	electrical discharge machining
FDB	fully developed boiling
IG	inverse gaussian
LN	lognormal
MApE	mean absolute percent error
N	normal (gaussian)
PDF	probability density function
PL$_s$	smooth plate
PL$_m$	medium rough plate
PL$_r$	rough plate
RMSpE	root mean squared percent error

a set of adjusting parameters in order to improve the prediction for the total amount of heat due to certain degree of skewness present in current distributions. In fact, these heat partitioning models use expressions for the interfacial and the evaporative heat fluxes by means of D_b^2 and D_b^3, where a quadratic and cubic mean value, respectively, are preferable to be introduced instead of the squared and cubed arithmetic mean.

In order to help in the proper statistical characterization of the bubble size population, an experimental analysis of the bubble diameter distribution has been carried out in this work. After the selection of the proper statistical model for the bubble size distribution, a correlation for the width of the probability distribution function (i.e. standard deviation) has been fitted, based on the data available from the author's experimental set up. In addition, a new correlation for the mean bubble size has been developed, based on the current data as well as on available experimental data from other authors covering a wide range of experimental conditions. Therefore, an adequate selection for the population distribution shape and an estimation of its parameters should be easy to other researchers, yielding to the description of more accurate models.

2. Review of previous work and global strategies

Since the second quarter of the past century, many researchers have proposed different models and correlations with a minor or major grade of empiricism, dealing with bubble sizing and some general trends have been established. On the determination of the bubble departure diameter, first work and effort of early researchers were summarized by Fritz [1] who gave an expression for the bubble diameter departing from a horizontal surface (Eq. (1)) contained in a liquid pool. This first force-based model formulates the equilibrium between the bubble buoyancy and adhesive forces to the wall, introducing the main role played by the capillary length in boiling processes.

$$D_b = 0.0208 \hat{A} \cdot \theta \ \hat{A} \cdot l_c \quad (1)$$

Due to the major limitation of Fritz's experiments, namely the use of air to model the vapor phase, several authors modified the Fritz expression in order to obtain better estimations for the bubble diameter. For instance, Zuber in 1959 [2] considered the existence of the superheated thermal layer between the bubble and the wall in the growing process (Eq. (2)) and Han and Griffith [3] in 1962 basically gave a different constant for the expression proposed by Fritz (Eq. (3)).

$$D_b = \left[l_c^2 \frac{6k_L(T_w - T_{sat})}{q_w} \right]^{0.3} \tag{2}$$

$$D_b = 1.192\theta l_c \tag{3}$$

Cole in 1967 [4] modelled the multiplier taking into account the Jakob number referred to the wall superheat and the effect of pressure by means of the density ratio (Eq. (4)). This expression was modified a year later by Cole and Rohsenow [5] paying no heed to the wall superheating and the contact angle, simplifying the former expression but introducing a fluid dependent constant in the correlation (Eq. (5)).

$$D_b = \rho^* \cdot Ja_w \hat{A} \cdot \theta \ \hat{A} \cdot l_c \tag{4}$$

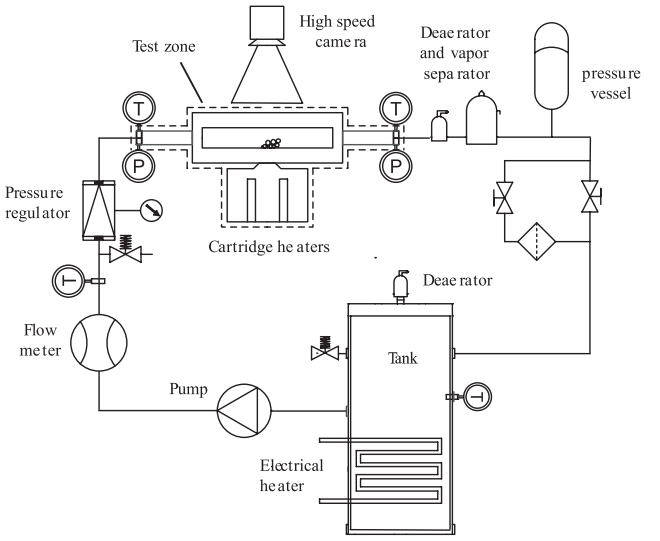

Fig. 1. Experimental facility.

$$D_b = \min\left[C_{bw} \cdot \exp\left(\frac{T_b - T_{sat}}{\Delta T_{ref}} \right), D_{b,max} \right] \text{ where } \begin{cases} D_{b,max} = 1.4 \text{ mm} \\ C_{bw} = 0.7 \text{ mm} \\ \Delta T_{ref} = 45 \text{ K} \end{cases} \tag{6}$$

cover the authors' data range, p: 0.1 to 1 MPa, $\Delta T_{sub}: 5-60$ K, $v_b: 0.08-0.2 \ \frac{m}{s}$ and $q = 0.47 \ \frac{MW}{m^2}$

$$D_b = C\hat{A} \cdot \rho^{*1.25} \cdot Ja_{sat}^{1.25} \hat{A} \cdot l_c \tag{5}$$

The above expressions were developed for pool boiling. In 1970 Tolubinsky and Kostanchuk [6] considered the bulk temperature dependence and gave an empirical expression (Eq. (6)) to be used in a particular range of pressure, flow velocity and liquid subcooling. Later in 1976, Unal [7] developed a semi-mechanistic model based on the thermal equilibrium for the bubble that is, considering both the evaporation inside the thermal boundary layer as well as the condensation in the outer region.

Kocamustafaogullari [8] modified Fritz's expression almost 50 years later including the density ratio effect in his pool correlation and changing the constant term (Eq. (7)). Farajisarir, as shown in his thesis in 1993 [9], assumed a dependence of bubble diameter with Jakob number and the degree of liquid subcooling (Eq. (8)).

$$D_b = 2.64 \times 10^{-5} \cdot \theta \hat{A} \cdot l_c \hat{A} \cdot \left(\frac{1}{\rho^*} - 1 \right)^{0.9} \tag{7}$$

$$D_b = 10.02 \times 10^9 \cdot \frac{\rho_L \alpha_L^2}{\gamma} \hat{A} \cdot \left(\frac{\rho^*}{Ja_w \hat{A} \cdot T^*} \right)^{1.65} \tag{8}$$

In 2002, Prodanovic et al. [10] proposed the boiling number as additional dimensionless magnitude in addition to Farajisarir assumptions to retain other possible dependences, as the flow velocity, in their correlation (Eq. (9)).

$$D_b = 236.749 \cdot \frac{\rho_L \alpha_L^2}{\gamma} \hat{A} \cdot Ja_w^{-0.581} \hat{A} \cdot T^{*-0.8843} \hat{A} \cdot \rho^{*1.191} \hat{A} \cdot Bo^{0.138} \tag{9}$$

Since 2005, an empirical expression due to Basu et al. [11] is widely used. In his thesis [12], Basu developed not only an expression for the bubble diameter (Eq. (10)), but a complete set to model the heat flux during subcooled boiling process.

$$D_b = 1.3\hat{A} \cdot l_c \hat{A} \cdot (\sin \theta)^{0.4} \hat{A} \cdot \left[0.13\exp\left(-1.75 \times 10^{-4} Re_{D_{hyd}} \right) + 0.005 \right] \left(\frac{Ja_w}{\rho^*} \right)^{0.45} \exp\left(-0.0065 \hat{A} \cdot \frac{Ja_{sub}}{\rho^*} \right) \tag{10}$$

Again in 2015, Brooks and Hibiki [13] also included the Prandtl number referred to saturation conditions in their correlation (Eq. (11)), in order to capture a wide range for the transport properties and the effect of other refrigerants apart from water. They also gave two different multipliers for the correlation, one for conventional channels and the other to use with mini channels. According to previous works, they accept a characteristic length of 3 mm for the limit between mini and conventional channels, but due to the limited data available they only gave a different scale for each morphology.

$$D_b = K\hat{A} \cdot l_c \hat{A} \cdot Ja_T^{-0.49} \hat{A} \cdot \rho^{*-0.78} \hat{A} \cdot Bo^{0.44} \hat{A} \cdot Pr_{sat}^{1.72} \quad \text{where} \quad \begin{cases} K = 2.11 \times 10^{-3} (\text{conventional channels}) \\ K = 1.36 \times 10^{-2} (\text{mini channels}) \end{cases} \tag{11}$$

In summary, among the different approaches used to address the modelling of the bubble diameter several conclusions can be extracted.

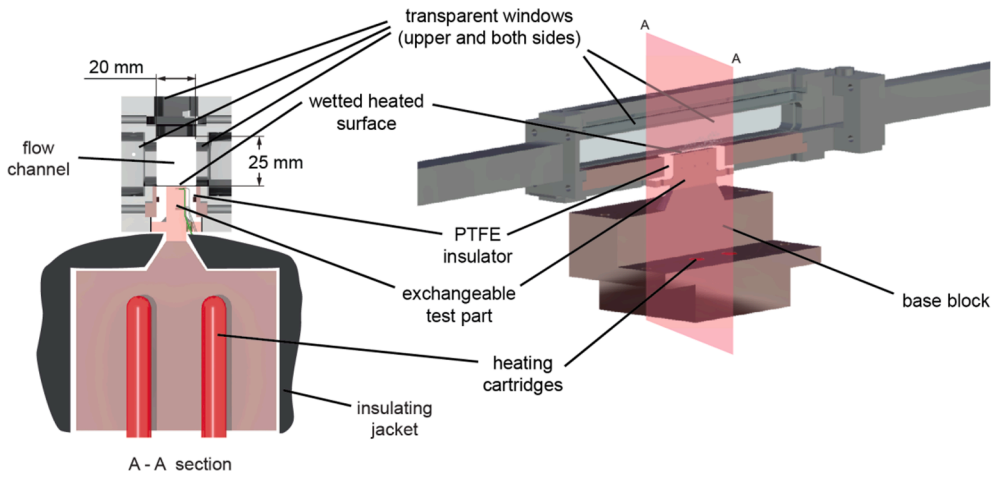

Fig. 2. Test zone and flow channel details.

Table 1
Test matrix.

Condition	Pressure [kPa]	Bulk temperature [°C]	Subcooling degree [°C]	Bulk velocity [m/s]	G [kg/m^2/s]
1	150	76.5	34.8	0.50	487.0
2	125	80.0	26.0	0.25	241.3
3	175	80.0	36.0	0.25	241.3
4	125	80.0	26.0	0.75	724.0
5	175	80.0	36.0	0.75	724.0
6	150	85.0	26.3	0.10	96.9
7	110	85.0	17.3	0.50	484.3
8	150	85.0	26.3	0.50	484.3
9	190	85.0	33.6	0.50	484.3
10	150	85.0	26.3	0.90	871.8
11	125	90.0	16.0	0.25	243.0
12	175	90.0	26.0	0.25	243.0
13	125	90.0	16.0	0.75	728.9
14	175	90.0	26.0	0.75	728.9
15	150	93.5	17.8	0.50	481.5

At the beginning, pool saturated boiling expressions for the bubble diameter were based on a balance based on both the buoyancy and the surface tension forces. After the first proposed models, researchers started to tackle the problem also under an energy approach and the superheating degree started to be considered. Moreover, with the inclusion of the subcooling degree, the previous expressions were adapted to work in subcooled conditions. In order to get a solution for flow boiling, the Reynolds number began to be used to characterize the effect of the flow velocity in the bubble detachment process. Several authors have been used the boiling number instead, based on a better error figure in their models. Concerning the contact angle, many authors avoid using it in correlations since the difficulty of its measurement and characterization, even worsened by the stochastic effect of the flow on the bubble.

3. Experimental setup

3.1. Test bench and measure equipment

A basic sketch of the experimental facility including the main elements is shown in Fig. 1. The system can be divided into two parts, the test area and the remaining subsystem allowing the control and the proper adjustment of bulk temperature, pressure, and volumetric flow rate. The test section, boxed with dashed line, comprises the wall heating system and the boiling surface. The AISI-316 flow duct through this section is 20 × 25 mm cross-sectional and 1200 mm length. A clarifying illustration for this zone is shown in Fig. 2. To determine the experimental value for the bubble diameters, a 10,000-fps speed camera with a sensor resolution of 400 × 170 pixel is used together with a couple of high luminous flux LED lamps. Because of brevity, additional aspects concerning the equipment features and experimental facility are omitted here but the reader can easily consult previous work from the authors [14], running experiments in the same bench. Additionally, the basis and an extensive description for the bubble recognition algorithm is available in [15,16].

Table 3
Uncertainties.

Variable	Assumed tolerances	Error@FDB (low activity)	Error@FDB (high activity)
T_b	±0.35 K	–	–
v_b	±4.6 mm·s^{-1}	–	–
p	±3000 Pa	–	–
D_b	±0.029 mm	–	–
T_{sat}	±1.21 K	–	–
k	±0.204 W·m^{-1}·K^{-1}		
T_{1x}, T_{2x}	±0.85 K		
T_Δ	±1.20 K		
x_Δ	±0.6 mm		
x_w	±0.35 mm		
T_w	–	±0.82 K	±2.16 K
q_w	–	±51.8 kW (±14.7%)	±80.2 kW (±7.4%)

Table 2
Morphological description of after-tested parts.

Designation	Surface finish	S_a [μm]	S_{dr} [−]	$\overline{R_{a,x_{min}}}$ [μm]	$\overline{R_{a,x_{max}}}$ [μm]	$\overline{R_{a,y_{min}}}$ [μm]	$\overline{R_{a,y_{max}}}$ [μm]
PLs	Sanded	0.37	0.47%	0.27	0.37	0.30	0.43
PLm	EDM + Sanded	1.44	1.33%	0.85	2.51	0.83	2.34
PLr	EDM	7.66	16.21%	7.11	7.96	6.78	7.67

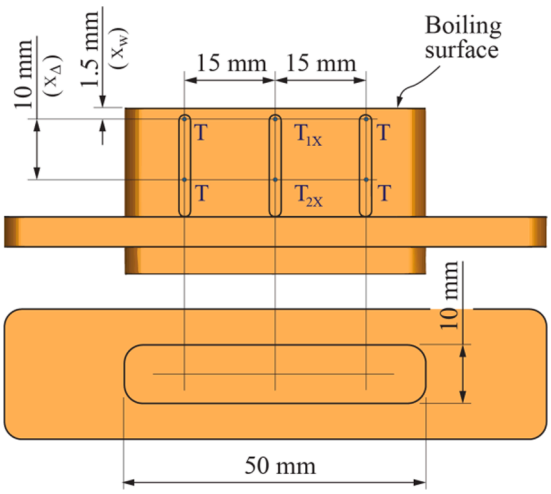

Fig. 3. Test part functional dimensions.

3.2. Test matrix and methodology

A central composite matrix of experiments was designed to evaluate the different response of boiling parameters to changes in five levels of temperature (from 76.5 to 93.5 °C), pressure (from 110 to 190 kPa) and velocity (from 0.1 to 0.9 m/s). The resulting test matrix comprising the selected 15 conditions, is listed in Table 1.

Once the primary condition was set, heat flux was varied, in steps of 50 kW/m^2, to cover the range between 200 and 650 kW/m^2 for each single condition. The entire test matrix was repeated for the three different copper surfaces (Table 2). All the surfaces are sized the same (10 × 25 mm) but different surface finishing was used to discern a different performance. One of the surfaces was prepared using sandpaper to get a commercial smooth surface of about 0.4 μm of roughness. The other two were spark eroded with EDM, to get more than 7 μm, one of which was finally sanded to obtain a mixed behavior in between the other two. The morphological features of the three parts are summarized in Table 2. Here, the classical 2D amplitude parameter R_a is given along with its 3D equivalent S_a, and the hybrid parameter S_{dr} namely developed interfacial area ratio and explained after in the text. For the sake of brevity, only roughness figures measured just after the tests with a Wyko NT1100 profilometer are shown in the table. The reader will find additional details on the topographic study of the three parts as well as on the heated surface ageing process in references [1517].

The uncertainties assumed in this work have been calculated using the classical theory of propagation of uncertainty. According to the available tolerances given by the manufacturer for the different experimental apparatuses, considering the manufacturing process tolerances and after the calibration of the thermocouples, the values for the assumed uncertainties are shown in Table 3. For instance, the wall temperature uncertainty is calculated with the Eq. (12). Because it depends on the magnitude of the measured property, in the table is shown its value for two characteristic points as reference. As inferred from Eqs. (12)–(14), wall temperature is calculated by extrapolation, after reading the temperatures T_{1x} and T_{2x} (Fig. 3) and calculating the heat flux. The latter, is calculated by reading the values of the thermocouples (k-type, class-2 tolerance, 0.5 mm diameter and 0.03 s response time) embedded in the test part and arranged as shown in Fig. 3. Although three pairs have been mounted, only the values T_{1x} and T_{2x}, located in the recorded area, are used for heat flux calculation assuming Fourier's law. The other sensors are mounted for homogeneity temperature field checking purposes.

The adopted machine vision algorithm is based on a pattern recognition concerning the two bright spot areas that will become visible after illuminating the bubbles with two diametrically opposed light sources. This algorithm analyses the top view and uses several criteria (level of brightness, centroids distance, area ratio, etc.) to determine if two twin bright areas belong to the same bubble or not. Further information about the recognition and bubble tracking process is deeply described in [15,16]. The optical system calibration was checked before each batch of tests by means of a metal sheet with graduated marks and little controlled steel balls. Since the relative distance between the camera and the plate could undergo changes due to mounting tolerances the pixel per mm ratio of the machine vision system was registered before each recording session. The bubble diameter tolerance is the maximum expected since it is based on the lowest ratio encountered which was 17.1 px/mm.

$$\xi_{T_w} = \left[\xi_{T_{1x}}{}^2 + \left(\frac{\partial T_w}{\partial x_w}\right)^2 \xi_{x_w}{}^2 + \left(\frac{\partial T_w}{\partial q_w}\right)^2 \xi_{q_w}{}^2 + \left(\frac{\partial q_w}{\partial k}\right)^2 \xi_k{}^2\right]^{0.5} = \left[\xi_{T_{1x}}{}^2 + \left(\frac{q_w}{k}\right)^2 \xi_{x_w}{}^2 + \left(\frac{x_w}{k}\right)^2 \xi_{q_w}{}^2 + \left(\frac{q_w x_w}{k^2}\right)^2 \xi_k{}^2\right]^{0.5} \quad (12)$$

$$\text{where } \xi_{q_w} = \left[\left(\frac{\partial q_w}{\partial k}\right)^2 \xi_k{}^2 + \left(\frac{\partial q_w}{\partial T_\Delta}\right)^2 \xi_{T_\Delta}{}^2 + \left(\frac{\partial q_w}{\partial x_\Delta}\right)^2 \xi_{x_\Delta}{}^2\right]^{0.5} = \left[\left(\frac{-T_\Delta}{x_\Delta}\right)^2 \xi_k{}^2 + \left(\frac{-k}{x_\Delta}\right)^2 \xi_{T_\Delta}{}^2 + \left(\frac{kT_\Delta}{x_\Delta{}^2}\right)^2 \xi_{x_\Delta}{}^2\right]^{0.5} \quad (13)$$

$$\text{and } \xi_{T_\Delta} = \xi_{(T_{1x}-T_{2x})} = \left[\left(\frac{\partial T_\Delta}{\partial T_{1x}}\right)^2 \xi_{T_{1x}}{}^2 + \left(\frac{\partial T_\Delta}{\partial T_{2x}}\right)^2 \xi_{T_{2x}}{}^2\right]^{0.5} = \sqrt{2}\xi_{T_{1x}} \quad (14)$$

4. Results and discussion

4.1. Bubble size distribution

In the early years of boiling processes characterization, the generalized shape assumed for the bubble size distribution was a normal distribution. With the improvement of the visualization techniques and measuring methods, the Gaussian distribution was turning into a more skewed distribution depending on the experimental conditions [18]. Nowadays, it is a recently proved fact by many researchers, as Colgan et al. [19] and Ooi et al. [20], that the bubble diameter population follows a left skewed distribution within the low pressures range. Martinez-Cuenca et al. [21] shown that all their sample meet with a generalized lognormal distribution. Kaiho et al. [22] concluded that the gamma distribution shows a much better agreement with experimental data than the normal distribution.

For the presented data, the lognormal (LN), inverse Gaussian (IG), gamma and Weibull probability density functions were tried. Although the current sample was found to be clearly left skewed, the normal (N) distribution has also been included in the comparison since its historical use. As the entire sample for each plate is used here, the same normalizing approach for the bubble diameter as in the work of Martinez-Cuenca et al. [21] was used. Therefore, all the diameter samples have been normalized by means of the average diameter for each individual condition. After processing more than 940,000 bubbles using machine vision techniques, both the lognormal and the inverse Gaussian probability distribution were found the best options to fit the experimental data of the three plates (Fig. 4). These probability functions are closely related to combinations of random and stochastic processes and present a very similar fitting error (Table 4).

The aim of Fig. 4 is to illustrate the best generalized options to fit experimental data. A complete table with the errors for each individual condition (i.e. plate, condition and heat flux) is included in the annex for both the lognormal and the inverse Gaussian fitting models (Table A2).

At the sight of the results, both a generalized lognormal or inverse Gaussian probability models can accommodate the normalized bubble size distribution for the current experimental sample and every plate as a

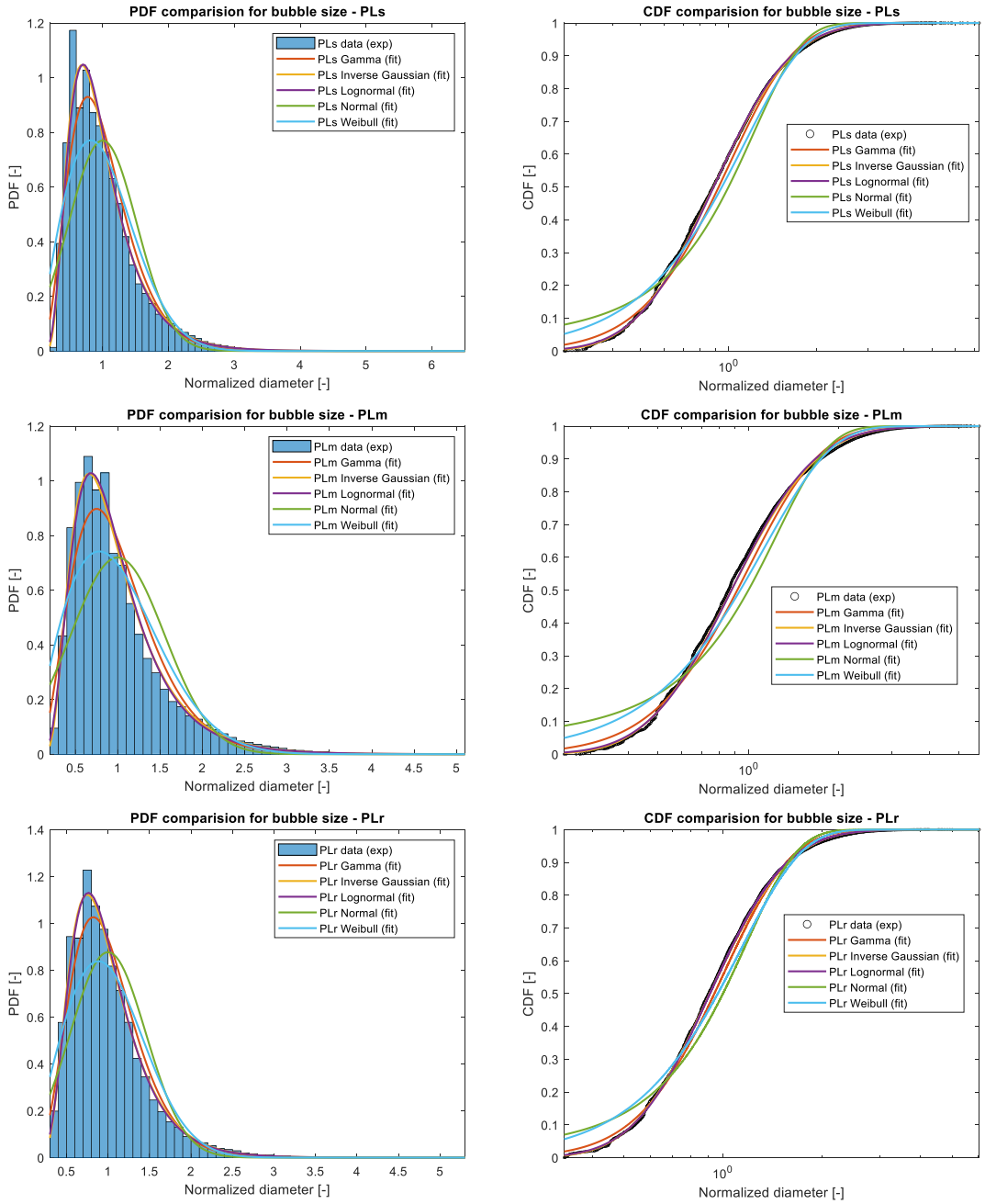

Fig. 4. Comparison of several distribution functions (Lognormal, Inverse-Gaussian, Weibull, Gamma and Gaussian) for the whole experimental sample and the three plates (Up: smooth plate; middle: medium plate; bottom: rough plate).

Table 4
CDFs comparison for the samples as a whole.

Plate / sample size	Error index	Gamma	Inverse Gaussian	Lognormal	Normal	Weibull
PLs	MApE	4.5%	1.1%	1.4%	19.5%	8.6%
452414	R squared	0.9905	0.9994	0.9990	0.9489	0.9714
PLm	MApE	8.3%	2.6%	3.1%	26.9%	17%
357888	R squared	0.9815	0.9972	0.9971	0.9072	0.9601
PLr	MApE	6.4%	1.8%	2.0%	19.5%	16.0%
136986	R squared	0.9920	0.9994	0.9995	0.9489	0.9700

whole. In order to analyze the physical dependences and the most likely causes for the variability of experimental data, a study concerning the standard deviation of each individual condition is necessary.

Prior to conduct an analysis, a probability model has to be chosen. The resulting variances for the different individual size distributions, that is grouped by plate, condition and heat flux, show no significant difference between the lognormal and the inverse Gaussian models for the normalized diameter (Fig. 5). This agreement between both models

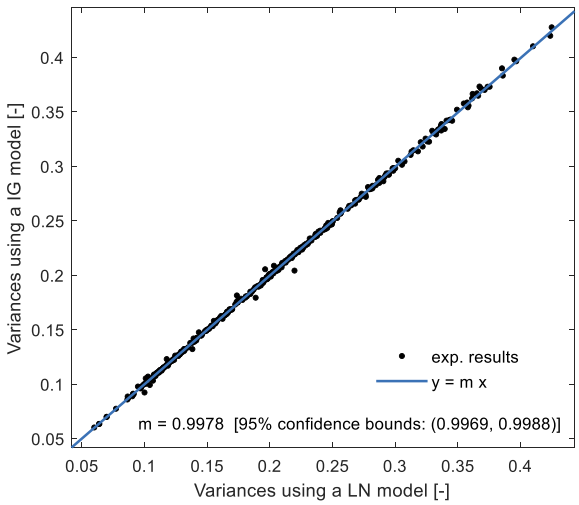

Fig. 5. Variances using an inverse Gaussian model vs. variances using a lognormal model. Individual sample fittings grouped per plate, condition, and heat flux.

is not new and was proved by several researchers in the past over a wide range of applications [23–25]. This affirmation is only valid under a certain range for the coefficient of variation (CV) that is, the standard deviation to mean ratio. According to Takagi et al. [23], the agreement between the inverse Gaussian and the lognormal is easily analytically checked provided that the CV is smaller than the unity. All the bubble size samples of this work meet with the previous condition since the CV ranges between 0.24 and 0.65 with an averaged value of 0.44.

Nevertheless, the lognormal distribution is selected in this work since other researchers [21] have successfully used it before with bubble diameter samples in nucleated boiling. Generally speaking, the inverse Gaussian (Eq. (15)) is closely related with life-time studies and frequencies [25] whereas the lognormal distribution accommodates a wide range of growing and sizing physical and biological processes [26]. In addition, this distribution can be easily converted in a Gaussian PDF, by means of the log-to-natural domain transformation, allowing the obtaining a proper standardized form.

$$f\left(\widehat{D}\right) = \sqrt{\frac{\lambda}{2\pi\widehat{D}^3}}\exp\left[\frac{-\lambda\left(\widehat{D}-\mu\right)^2}{2\mu^2\widehat{D}}\right] \tag{15}$$

The most common parametrization for the lognormal distribution and the one used here, is shown in Eq. (16). In this expression, μ and σ are the parameters for the log-normal PDF parametrization, and they are also provided in the table of the annex for the three plates and all the experimental conditions and heat fluxes (Table A2). Comparing this expression with the Gaussian PDF definition, μ and σ are straightforwardly found to be the mean and the standard deviation of the corresponding sample after taking logarithm.

$$f\left(\widehat{D}\right) = \frac{1}{\widehat{D}\sigma\sqrt{2\pi}}\exp\left[\frac{-\left(\log\widehat{D}-\mu\right)^2}{2\sigma^2}\right] \tag{16}$$

4.2. Sample size

To improve the individual analysis, a simple study on how the sample size affects the goodness of fit was performed. Depending on the thermo-fluid dynamic conditions for each of the 15 experimental points, not all the samples for all the covered heat flux range might be appropriate. Of course, this is not true for the analysis of the whole sample with hundreds of thousands of bubbles for each plate but can led to

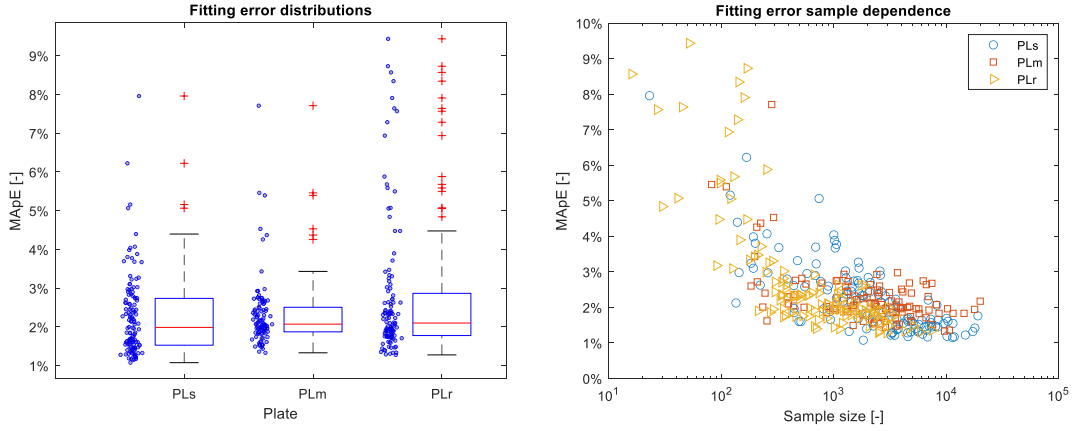

Fig. 6. Fitting error. Left: box plots for the error distributions, right: error vs. sample size.

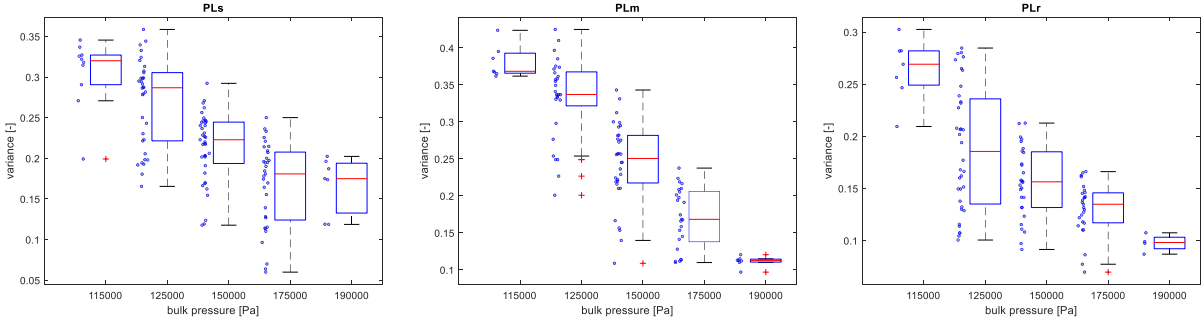

Fig. 7. Variance of the normalized distributions vs. bulk pressure. Left: smooth plate, middle: medium plate and right: rough plate.

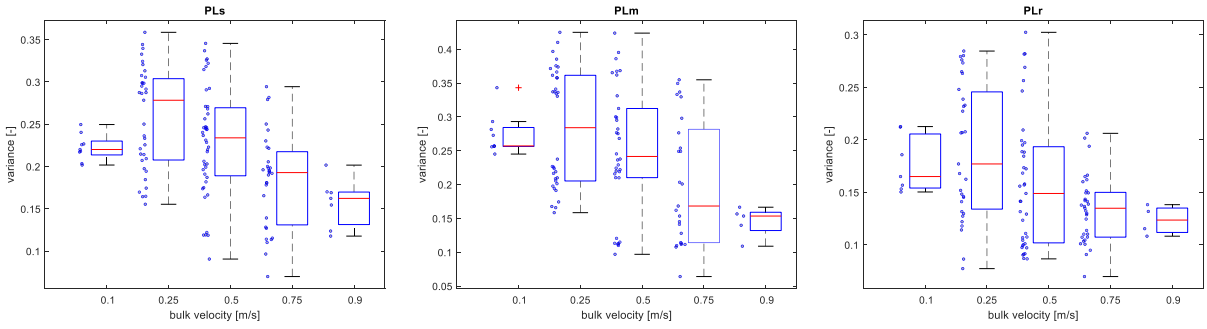

Fig. 8. Variance of the normalized distributions vs. bulk velocity. Left: smooth plate, middle: medium plate and right: rough plate.

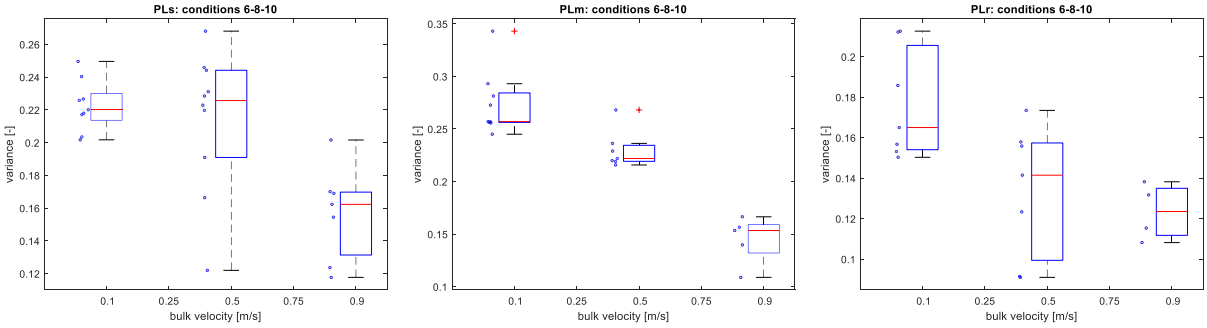

Fig. 9. Variance of the normalized distributions vs. bulk velocity (test conditions: 6, 8 and 10). Left: smooth plate, middle: medium plate and right: rough plate.

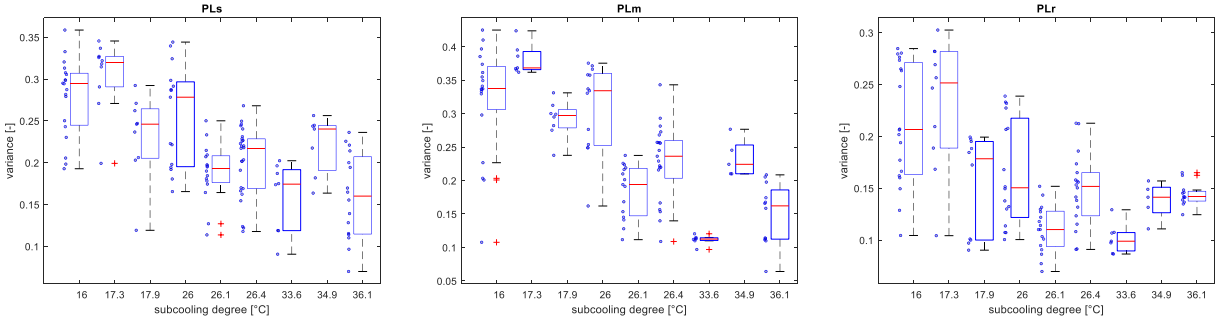

Fig. 10. Variance of the normalized distributions vs. subcooling degree. Left: smooth plate, middle: medium plate and right: rough plate.

misleading results if the sample significantly reduces its size.

Once the lognormal model is accepted the fitting errors can be calculated for each plate, condition, and heat flux. The error is below 3% when the sample rises above 300 bubbles (Fig. 6, right) for the three plates and the majority of conditions. The reader can consult the sample size for each of the conditions tested given in ~~the~~ Table A1, to figure out a value for the fitting error at every single condition. To give a global perspective, the error for the distributions is box-plotted in the left chart of Fig. 6 and given in the annex as previously mentioned (Table A2). The outliers present in the sample, red crossed points, will be removed in the subsequent analysis.

4.3. Dimensional dependences of the variance

After identifying and rejecting outliers of the error distributions, a study of the dimensional dependence of the normalized distribution widths has been carried out. The selected primary variables were the bulk pressure, bulk velocity and the wall heat flux and wall temperature. Concerning the thermal state both the superheating and the subcooling degrees have also been included. In accordance with previous studies [21,22], the standard deviation of the bubble size distributions rises with the mean diameter. There are two main sources increasing the variability of the bubble size population associated with the temperature and flow randomness. For isolated bubbles, and when the bubble is growing at the nucleation site, the fluctuations of local wall temperature and superheating will affect to its size. After that, and if the conditions allow the sliding of the bubble, the stochastic nature of the flow velocity may significantly affect the subsequent bubble growth and detachment process. Moreover, the roughness and morphology may influence the bubble from wall detachment and lastly, with an enough number of bubble present, the merging process will increase the size of certain bubbles.

The strongest effect in the variance of the experimental distributions is due to the pressure since it resolves the energy reference by means of the saturation temperature. A clear effect can be seen in ~~the~~ Fig. 7, where the variance clearly diminishes as the pressure rises for the three plates. A possibility could reside in the rise of the easiness for the bubbles to grow as the pressure diminishes, increasing the probability of finding new and a broader range of diameters. Moreover, according to the heterogeneous nucleation theory, the amount of energy to pre-activate

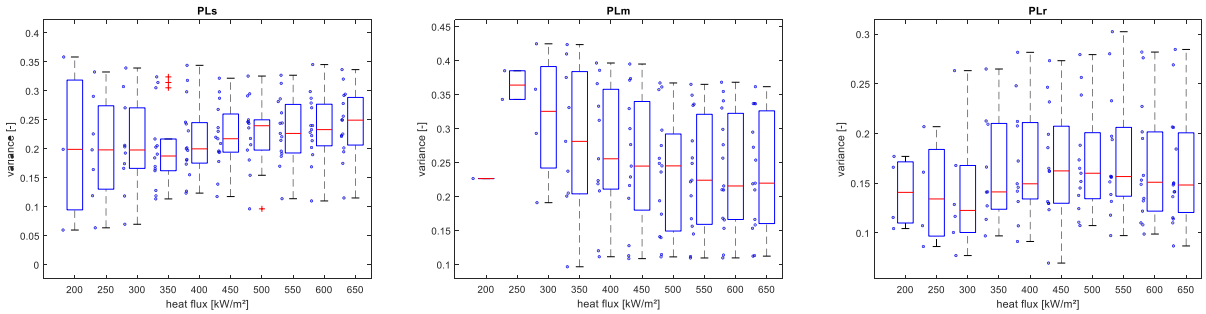

Fig. 11. Variance of the normalized distributions vs. wall heat flux. Left: smooth plate, middle: medium plate and right: rough plate.

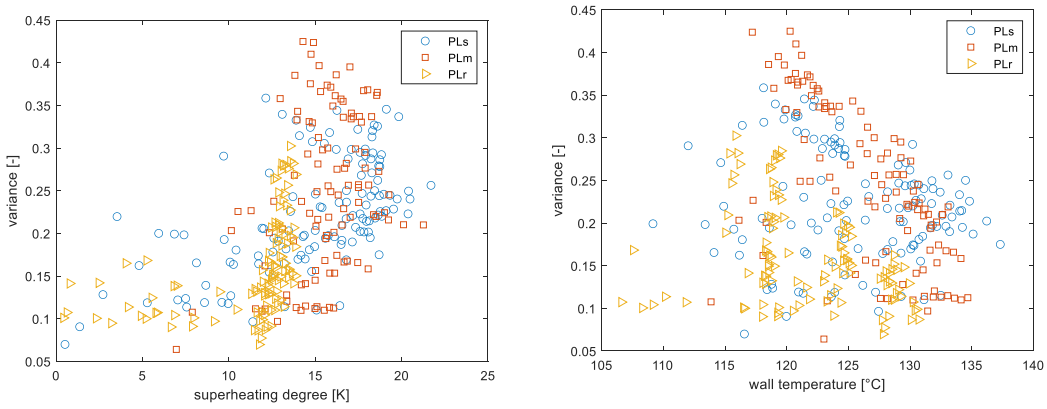

Fig. 12. Variance of the normalized distributions vs. wall superheating degree (left) and vs. wall temperature (right).

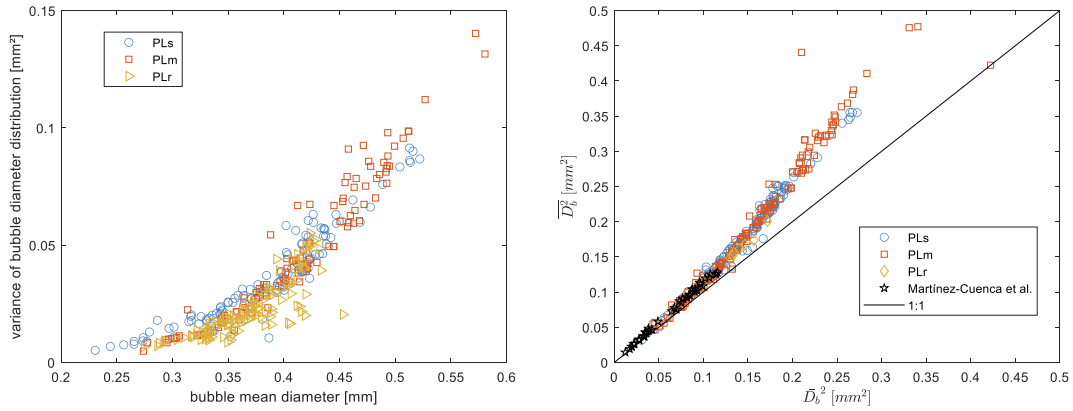

Fig. 13. Left: Variance of the bubble diameter individual distributions vs. bubble mean diameter for the three plates (dimensional values). Right: Mean squared diameter vs. mean diameter squared for the three plates and data from [21].

nucleation sites is lower since the saturation temperature is lower for the same bulk temperature. Therefore, a broader range of nucleation cavities are available to nucleate and then the range of population sizes is expected to be higher. Also, since bigger bubbles are present, these are more exposed to the turbulent core of both the thermal and hydrodynamic boundary layers, increasing again the randomness in the population, making a wide-ranging subcooled liquid or quenching effect.

The effect of the velocity on the variance can be seen in Fig. 8. The variance diminishes with the velocity for the three plates, but this reduction effect is not so strong as the case with the pressure growth. The suppression effect of the flow velocity on boiling activity causes both reduction in size and population, yielding to narrower distributions. Isolating the conditions for those where the velocity is the only variable (Fig. 9), i.e. experimental conditions (6), 8 and 10, the velocity effect becomes vague at the low velocity range and the smooth plate. Nevertheless, for the medium and roughest plates, this trend passes unnoticed. This result points out the necessity of further work on the influence of the morphology in the extremely complex detachment process and on the competition between the contact forces versus drag forces. According to Kandlikar and Stumm [27] the advancing and receding contact angles passes through a minimum and a maximum respectively in the low-mid range of velocities and low-pressure flow. For the smooth plate this could be part of the explanation of the observed trend. The other two plates, with significantly deeper cavities than the smoothest one, the influence of the flow drag at those velocity range is weaker and remains unperceived.

Concerning the subcooling degree (Fig. 10), the observed effect for the current experimental sample is the inhibition of bubble formation as the subcooling degree rises because the quenching effect becomes more efficient. This bubble production due to a higher subcooling is also

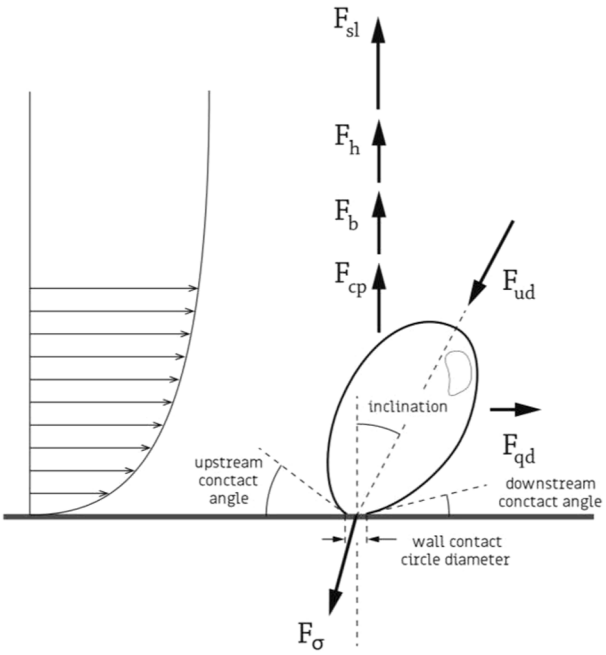

Fig. 14. Forces influencing the bubble departure phenomenon according to Klausner et al. [18].

combined with the effect of getting thinner boundary layers [28], since the bubble condensation process at the top is likely to act as a size limiting factor, making the sample more uniform and diminishing the variance.

The dependence of the variability with the heat flux (Fig. 11) seems to be negligible when all fluxes and plates are considered. The behavior at low heat fluxes for each individual plate can mislead the analysis but the so low number of bubbles present at low heat fluxes, does not support any conclusion for those range. Several authors in the past ([6,10]) did not observed any significant effect of the heat flux on the bubble growing process, and Maurus et al. [29] observed a very weak dependence of the heat flux in small bubbles size. In this work the variance is likely to scale this behavior and no clear influence has been achieved. Moreover, regarding the different trend between the three plates any common conclusion on that aspect should not be trustworthy.

Finally, the effect of the superheating degree and the wall temperature is shown in Fig. 12. As expected, the higher the difference between the wall temperature with respect to the saturation state of reference (Fig. 12-left), the higher the amount of energy to be transferred by means of boiling mechanism. In consequence, a broader range for the variance limits are encountered after a certain value for the superheating degree. The associated rise in the nucleation activity, the increase of bubble size, and considering the higher probability concerning bubble merging processes, yields to the widest distributions observed. Even so, and also when considering the wall temperature alone (Fig. 12-right), the scatter present in the current data does not allow to notice any clear effect as happened with the heat flux.

4.4. Dimensionless correlation for the variance

In addition to the dependences covered in the previous paragraph, it is very useful from a statistically point of view, to show the dependence of the variance with the bubble size itself, since most of the previous factors has also influence in the bubble size. Therefore, the variation of the variance against the diameter mean value is shown in ~~the~~ Fig. 13- left for the three tested plates and assuming a LN distribution. Due to the clear trend observed, the same factors having influence in the bubble size, that is the location of the distribution, are likely to govern the width or shape of the distribution. In consequence, a clear strategy to find a correlation for the variance has arisen. Among the little amount of published work, Martinez-Cuenca et al. [21], based on their observations, suggest a linear scaling of the standard deviation with the bubble size, that is, a constant coefficient of variation within the experimental range tested. They support their statement by means of the existence of a linear relationship between the mean diameter squared and the mean squared diameter. Current results are coherent in the low bubble size range, but the experimental sample shows a change in the scale factor beyond a certain size not covered by the previous authors (Fig. 13-right).

To model the growth and detachment process of the vapor bubbles, and in the end the maximum bubble size, several approaches (empirical, energy conservation, force balance, etc.) have been used. In 1993, Klausner et al. [18] presented a comprehensive study, based on a force balance, for the bubble departure in flow boiling and R113. Their work was afterwards extended and modified by several authors [33–40].

Klausner et al. assume the existence of the following forces (Fig. 14) acting on a bubble: surface tension force (F_σ), as a function of the wall contact circle diameter, the local contact angle and the surface tension; quasi-steady drag (F_{qd}), as a function of the time averaged velocity profile at the center of the bubble, diameter of the bubble, and the viscosity and mass density of the liquid; force due to asymmetrical bubble growth (F_{ud}), proportional to the mass density of the liquid, the bubble inclination angle, the bubble diameter, its growth rate and the rate of change of this growth rate; shear lift force (F_{sl}), estimated once the velocity profile near to the wall is assumed, by means of the mass density and viscosity of the liquid, the projected area of the bubble and the shear rate calculated employing the velocity profile; buoyancy force (F_b), as the floatability force exerted on bubble volume due to the two-phase mass density difference; the force due to the hydrodynamic pressure distribution on the bubble vapor-liquid interface (F_h); and the contact pressure force (F_{cp}), which is the force due to the pressure difference inside and outside the bubble on the dry area in contact with the wall. Using the Laplace-Young law, this last force can be expressed by means of the wall contact circle area, the surface tension, and the curvature of the bubble surface at the contact line. Also, after considering this last contact pressure force, the previous hydrodynamic pressure force can be

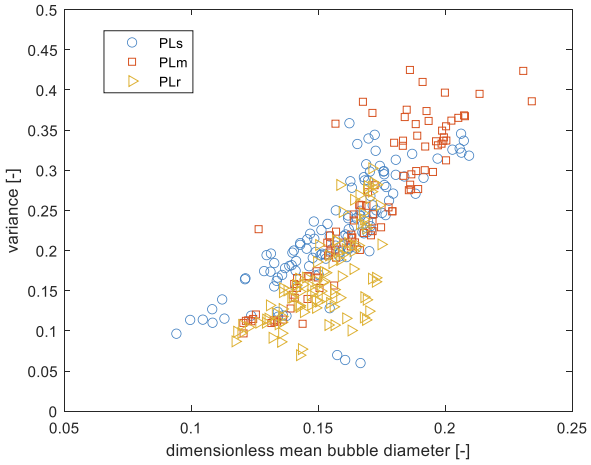

Fig. 15. Variance of the normalized distributions vs. non-dimensional mean bubble diameter.

estimated from the effect of the hydrodynamic pressure acting on an area equal to the wall contact circle but at the top of the bubble, providing that an axial symmetry for the bubble is assumed.

Regarding the force due to the bubble growth, Klausner et al. suggest the work of Mikic, Rohsenow and Griffith [41] to estimate the bubble growth rates. They derived expressions for the instantaneous bubble radius as a function of enthalpy of vaporization, superheating degree, density ratio, saturation temperature, wall Jakob number and liquid thermal diffusivity. Also, they included the dimensionless temperature difference as a subcooling factor for the case of having non-uniform temperature field as Steiner et al. [35] did later in their BDL model to account for the subcooling effect.

Also, to work out a representative value for some of these forces, an estimation on the time averaged velocity profile and the two-phase mean liquid velocity is needed. Under subcooled conditions, this problem can be tackled by means of the law of the wall and the averaged vapor quality to calculate the liquid two-phase velocity, that will be generally small or even negligible, depending on the subcooling degree. The wall shear stress needed by the law of the wall to calculate the shear velocity, may be modeled once the skin friction factor is assumed, estimated by means of the bulk flow velocity, mass density, viscosity, morphology of the wall and geometry of the heating channel. To find an approximate value for the void fraction, the evaporation heat flux commonly used in the wall partitioning heat flux models [11,42,43] derived on an energy approach basis could be employed. The evaporative heat flux is commonly model as the product of the latent heat associated to the volume of vapor of the arisen bubbles, that will obviously depend on the number of bubbles present and so, on the active site

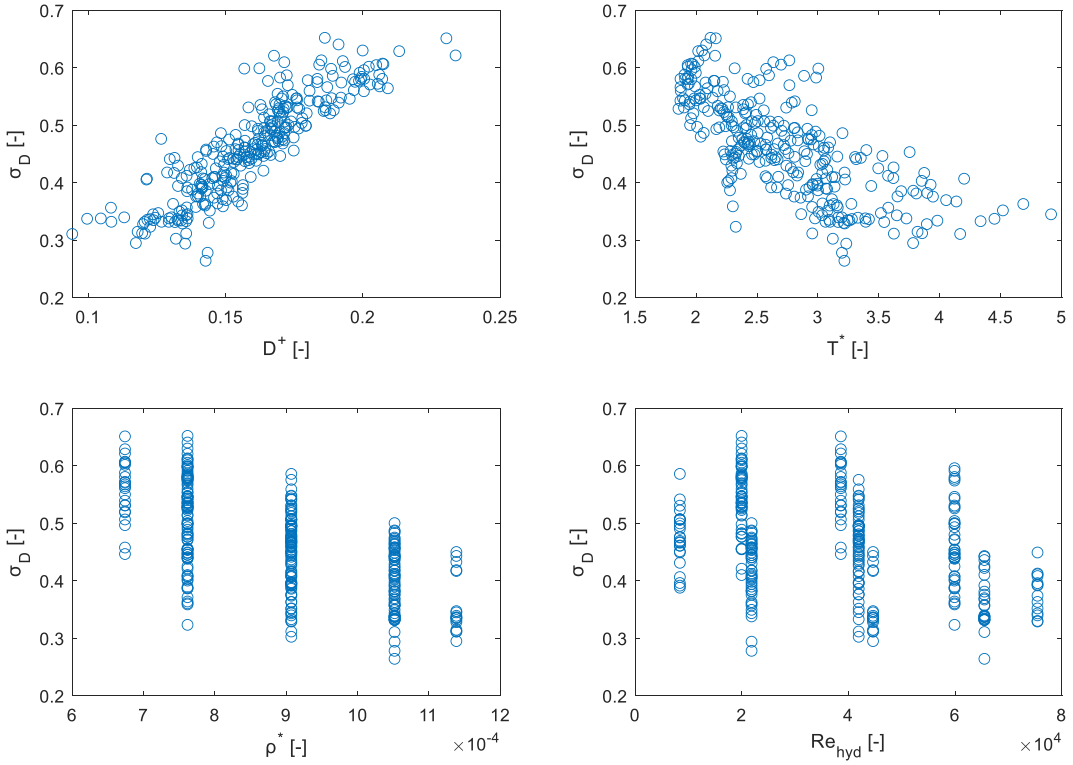

Fig. 16. Standard deviation of the normalized experimental sample against dimensionless diameter (top-left), dimensionless temperature difference (top-right), density ratio (bottom-left) and Reynolds number (bottom-right).

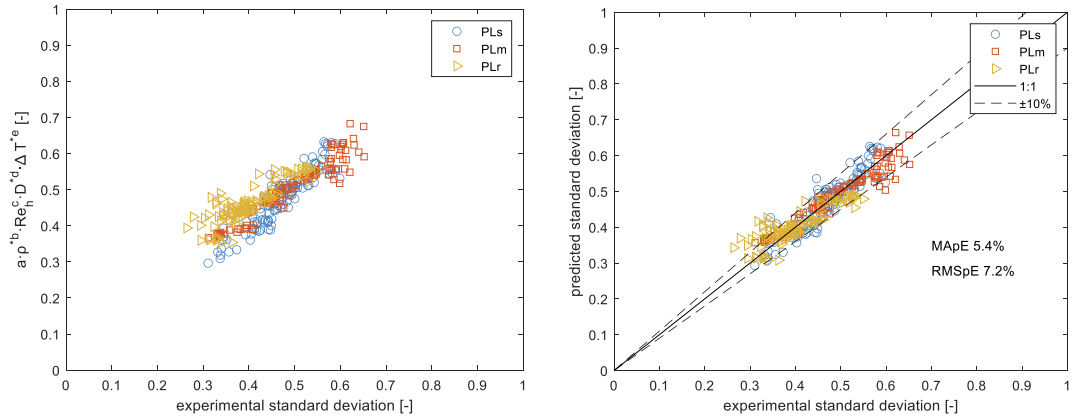

Fig. 17. Predicted standard deviation vs. experimental standard deviation. Left: correlation without the morphological term. Right: proposed correlation.

Table 5
Fitting results.

R^2	Adjusted R^2	MApE[a]	RMSpE[b]
0.8664	0.8642	5.4%	7.2%
Coefficient	value	t-statistic	p-value
a	0.643	3.11	0.0021
b	−0.25	−6.32	<0.0001
c	−0.063	−10.16	<0.0001
d	0.7	14.10	<0.0001
e	−0.12	−5.60	<0.0001
f	−0.45	−10.05	<0.0001

[a] $\mathbf{MApE} = \sum_1^N \frac{|y_{pred,i} - y_{exp,i}|}{y_{exp,i}}$

[b] $\mathbf{RMSpE} = \sqrt{\sum_1^N \left(\frac{y_{pred,i} - y_{exp,i}}{y_{exp,i}}\right)^2}$

density and nucleation frequency apart from the bubble mean diameter. The nucleation site density can be regarded as a function of the wall superheating degree and the bubble surface interaction [3144] and the nucleation frequency is generally built up considering a growth and a waiting time. According to Basu et al.'s model [11], the first one depends on both the wall and subcooled Jakob number as well as on the thermal diffusivity of the liquid, whereas the latter is a function of the superheating degree.

Among the above-described variables on which the mean diameter could depend on, there are several geometric variables, namely the contact angle distribution, the bubble inclination and instantaneous shape, or the wall contact circle; very difficult if not impossible, to be accurately measured. They are likely strongly influenced by the local random fluctuations of the flow properties as well as by the macro and micromorphology of the heating surface at the considered location. Therefore, the effects due to these variables will be lumped into an empirical coefficient to be experimentally determined.

In this work, based on the aforementioned considerations of the different forces and effects identified, the bubble diameter dependence is formulated as:

$$D_b = f\left(T_w - T_{sat}, T_{sat} - T_b, T_w - T_b, \rho_L, \rho_V, \rho_L - \rho_V, p, h_{LV}, c_{pL}, \alpha_L, \mu_L, \gamma, g, V_b, D_{hyd}\right) \quad (17)$$

As explained above, this functional dependence could be ~~hardly~~ improved with parameters concerning the bubble – wall interaction such us wall roughness and morphology, contact angle distribution and so on; but because of their measure is extremely difficult, this information is seldom included in databases.

Once the functional relationship (Eq. (17)) is assumed, the following dimensionless groups have been considered to characterize the bubble size dependence:

Table 6
Summary of experimental data.

Author	Heated surface material	Surface roughness [μm]	Channel Geometry	D_h[mm]	Orientation	Fluid	θ_{mean}[deg]
Klausner et al. (1993)[18]	Nichrome	N/A	Square[3]	25	Horizontal[a]	R113	40°
Thorncroft et al. (1998)[45]	Nichrome	N/A	Square	12.7	Vertical[d]	FC87	N/A
Prodanovic et al. (2001)[10]	S. Steel	N/A	Annular[1]	9.3	Vertical[c]	Water	58°
Basu (2003)[12]	Copper	N/A	Square	39.3	Vertical[c]	Water	30°
Situ et al. (2005)[46]	S. Steel	N/A	Annular[1]	19	Vertical[c]	Water	N/A
Okawa et al. (2007)[47]	Glass-ITO film	N/A	Annular	3	Vertical[c]	Water	45°
Murshed et al. (2010)[48]	S. Steel	N/A	Rectangular[2]	3.8	Vertical[c]	R134a	N/A
Yuan et al. (2011)[49]	Nichrome	6.4	Rectangular	3.85	Vertical[c]	Water	N/A
Chu et al. (2012)[50]	NiChrome + Fe	0.07	Annular[1]	22.2	Vertical[c]	Water	90°
Chen et al. (2012)[51]	Nichrome	6.4	Rectangular[2]	3.85	Vertical[c]	Water	N/A
Ahmadi et al. (2012)[52]	Copper	N/A	Rectangular	13.3	Vertical[c]	Water	18°
Sugrue et al. (2014)[53]	S. Steel	1.22	Rectangular	16.6	Horizontal[b]	Water	50°
Brooks et al. (2014)[1354–55]	S. Steel	N/A	Annular[1]	19	Vertical[c]	Water	57°
Ooi (2017)[56]	S. Steel	N/A	Square[2]	12.7	Vertical[c]	Water	N/A
Kaiho et al. (2017)[22]	Glass-ITO film	N/A	Rectangular	11.7	Vertical[c]	Water	14°
Colgan et al. (2019)[19]	S. Steel	0.197	Square[2]	12.7	Vertical[c]	Water	59°
Present data	Copper	0.4/1.4/7.4	Rectangular	22	Horizontal[a]	Water	80°

[a] Upward facing
[b] Upward and downward facing
[c] Upwards flow
[d] Upwards and downwards flow
[1] Wall temperature by Liu-Winterton
[2] Wall temperature by Chen-Butterworth
[3] Bulk temperature by Chen-Butterworth

Table 7
Experimental range covered by the dataset.

	Absolute pressure[kPa]	Bulk velocity $\left[\frac{cm}{s}\right]$	Mass flux $\left[\frac{kg}{sm^2}\right]$	Heat flux $\left[\frac{kJ}{sm^2}\right]$	ΔT_{sub} [K]	ΔT_w [K]	D_{hyd} [mm]	ρ^*	Bo	Ja_w	Pr_{sat}	T^*
Min. value	49.2	6.87	67.4	2.83	1.49	0.136	3.00	0.313e−3	0.0510 e−3	0.259 e−3	0.969	0.950
Max. value	1040	149	1443	1200	60.0	24.6	39.3	34.3e−3	3.01e−3	0.133	8.97	194

$$Eo = \frac{(\rho_L - \rho_V)gD_b^2}{\gamma} \quad Ja_{sub} = \frac{c_{pL}(T_{sat} - T_b)}{h_{LV}} \quad Ja_w = \frac{c_{pL}(T_w - T_{sat})}{h_{LV}} \quad Re_{hyd} = \frac{\rho_L V_b D_{hyd}}{\mu_L}$$

$$Pr_{sat} = \frac{\mu_L}{\rho_L \alpha_L} \quad T^* = \frac{T_w - T_b}{T_w - T_{sat}} \quad \rho^* = \frac{\rho_V}{\rho_L}$$

Since the density ratio scaled the pressure, the latter was omitted in the analysis. Also, the effect of the enthalpy of vaporization and the specific heat were lumped in the Jakob number as usual in boiling problems. Concerning the Jakob numbers, the reader should note the absence of the density ratio, as the latter has been considered as a dimensionless group itself. Additionally, the density difference effect is the one associated with the buoyancy force so the product $g(\rho_L - \rho_V)$ is the lumped functional group considered.

To select the dimensionless diameter of the bubble, the Eötvös number based in the bubble diameter (Eq. (18)) has shown the best agreement with experimental data. Particularly, this is the most widely dimensionless number used with the bubble diameter, where the ratio of the capillarity forces to the buoyancy ones are selected to be important.

$$\sqrt{Eo} = \sqrt{\frac{(\rho_L - \rho_V)gD_b^2}{\gamma}} = \frac{D_b}{l_c} = D^+ \tag{18}$$

Other authors like Prodanovic et al. [10], have been used the group $\frac{\gamma}{\rho_L a_L^2}$ to define the characteristic length, considering the thermal response to the temperature changes as the key factor. Additionally, using the Prandtl number and the previous groups, the group $\frac{\rho_L \nu^2}{g(\rho_L - \rho_V)}$ could be used instead where the viscous to floatability forces ratio need to be highlighted.

In ~~the~~ Fig. 15, the variance of the normalized distributions is plotted against the mean bubble size, where the strong correlation found in the dimensional version of the chart (Fig. 13-left) is again clearly visible.

After performing several trials among all the involved groups, the standard deviation is found to be a function of D^+, ρ^*, T^*, Re_{hyd} within the range of the current data. The observed trend with the different dimensionless groups is plotted in Fig. 16. As deduced from the previous figures (Fig. 13- left, Fig. 15) a large amount of the variability is expressed by means of the dimensionless diameter. At the sight of the results, some of the variability remains unexplained using only the diameter. It seems that the density ratio, Reynolds number and dimensionless temperature difference are capturing some additional effect mainly due to the pressure, bulk velocity and subcooling and superheating degrees.

In several past studies ([15,16]), a clear effect of the bulk surface morphology in the bubble diameter were identified. In this work, the different slope associated with the cloud points of the different plates (Fig. 17-left) after evaluating the other terms of the correlation, a remaining effect due to the different morphology of the three surfaces can be observed. After some regression analysis comparison, the hybrid surface parameter S_{AR} has been revealed as one of the best to accomplish the morphological dependence of the variance (Fig. 17-right).

The selected parameter S_{AR} was used by McHale and Garimella [30] in order to retain several effects of surface morphology in boiling systems. It was also successfully used in the past by the authors [31] to accommodate the dependence of the surface morphology in the active site nucleation density. S_{AR} is calculated as shown in Eq. (19) and derives from the normalized parameter S_{dr} defined in Eq. (20) and included in the ISO-25178 areal surface texture standard [32]. The reader should note here that the inclusion of this parameter only complements the morphological dependence of the variance of the bubble size distribution, but further work is still necessary to characterize the effect of other wall parameters as the contact angle distribution in the bubble detachment or the effect of the micromorphology on the shape of the contact line at the bottom of the bubbles. SinceS_{AR} is equivalent to the area ratio (actual or developed to projected area ratio) of the different surfaces, one possible explanation to the role played by the parameter could reside in the amount of available area to single phase convection. For instance, if both the smooth and the rough surfaces are evacuating the same amount of heat, the smooth one will need in general more and bigger bubbles and hence, the distribution will have a higher variance.

$$S_{AR} = \frac{S_{dr} + 100}{100} \tag{19}$$

$$S_{dr}(\%) = \frac{100}{A}\left\{\iint_A \left[\sqrt{1 + \left(\frac{\partial z(x,y)}{\partial x}\right)^2 + \left(\frac{\partial z(x,y)}{\partial y}\right)^2} - 1\right] dx \cdot dy\right\} \tag{20}$$

The final expression for the correlation is shown in Eq. (21) and plotted in Fig. 17-right. The Marquardt-Levenberg algorithm was the least squares method used to find the coefficients minimizing the sum of the squared differences between the observed and predicted values.

$$\widehat{\sigma_D} = a\hat{A} \cdot \rho^{*b}\hat{A} \cdot Re_{hyd}{}^{c}\hat{A} \cdot D^{+d}\hat{A} \cdot T^{*e}\hat{A} \cdot S_{AR}{}^{f} \tag{21}$$

The best fitting coefficients, several error index, t-statistic and p-value for the different coefficients are shown in Table 5. Despite of the little values for c, the term was kept in the correlation as it has found to be statistically significant and in accordance with the experimental trend observed.

4.5. Bubble size mean value

In this part of the work, a brief study about the mean bubble size encountered in flow boiling experiments running subcooled conditions is presented. At the end, a new correlation for the bubble mean diameter is obtained, covering a wide range of previously published experimental data as well as the current one, given in the annex (Table A1).

The compiled dataset about bubble diameter is summarized in Table 6 and the covered range by the whole dataset is shown in Table 7.

Since not all the authors give the wall temperature value in their respective dataset, a correlation value was used with a total of nine dataset. Two widely used correlations has been used depending on the geometry. With square and rectangular ducts, the famous correlation due to Chen [57] modified to subcooled conditions by Butterworth [58] was employed since, despite being more than 50 years old, it has found to be one of the most accurate with those geometries and stainless steel

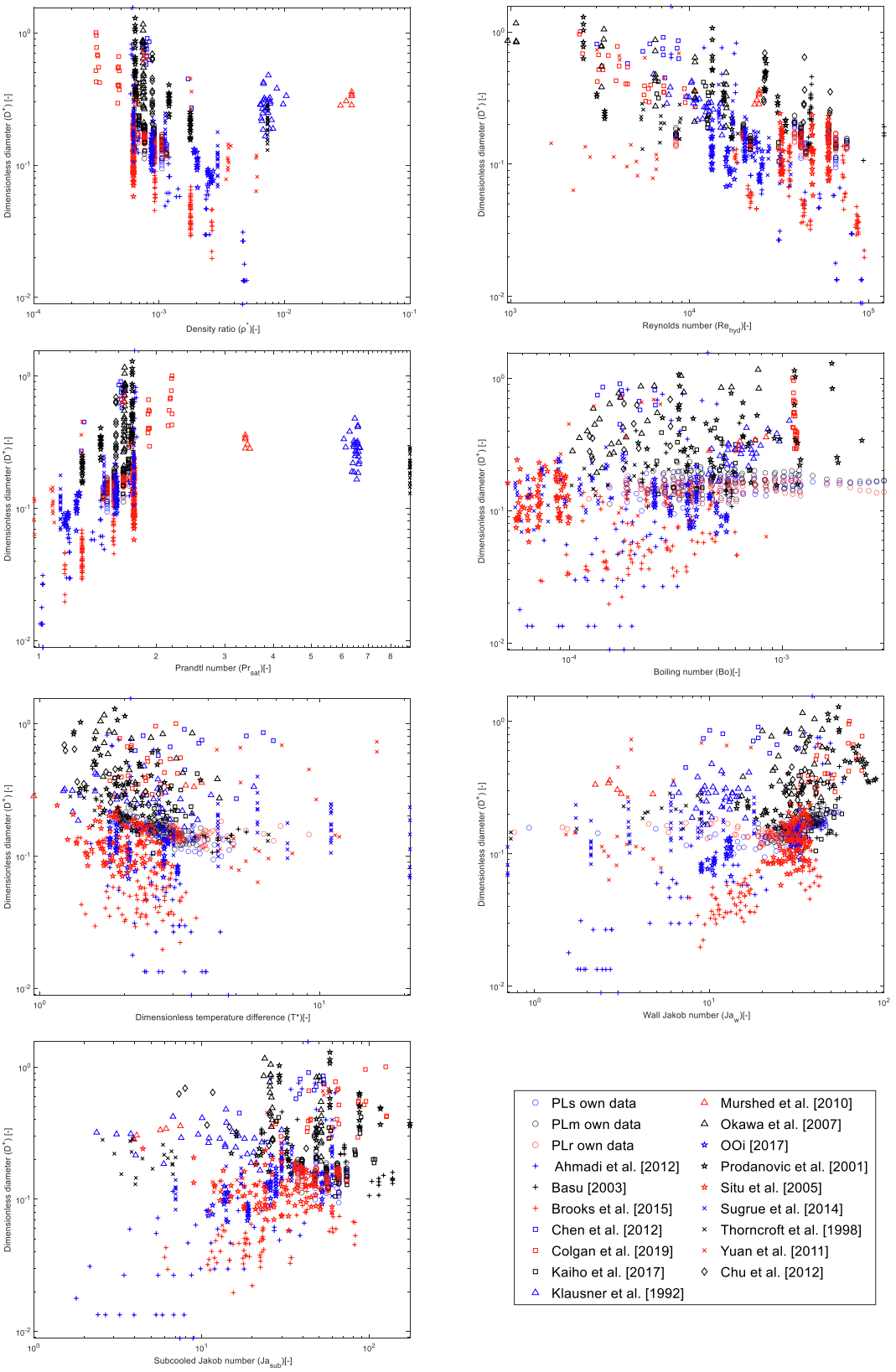

Fig. 18. Dependencies of the measured dimensionless mean bubble diameter and the selected dimensionless groups. Top-left: density ratio; top-right: Reynolds number; middle-up-left: Prandtl number; middle-up-right: boiling number; middle-down-left: dimensionless temperature difference; middle-down-right: wall Jakob number; bottom-left: subcooled Jakob number and bottom-right: common legend.

Table 8
Evaluation of selected models for bubble diameter.

Author	MApE [a]	RMSpE [b]
Fritz (1935) [c] [Eq. (1)]	82.0%	83.1%
Cole (1967) [c] [Eq. (4)]	608.4%	746.1%
Cole-Rohsenow (1969) [Eq. (5)]	349.9%	425.4%
Tolubinsky (1970) [Eq. (6)]	99.5%	245.1%
Kocamustafaogullari (1995) [c] [Eq. (7)]	2355%	2804%
Prodanovic (2005) [Eq. (9)]	93.2%	131.5%
Basu (2005) [c] [Eq. (10)]	139.0%	253.1%
Brooks-Hibiki (2015) [Eq. (11)]	33.0%	43.5%
Presented model [Eq. (22)]	28.9%	36.8%

[a] $\text{MApE} = \sum_1^N \frac{|y_{pred,i} - y_{exp,i}|}{y_{exp,i}}$

[b] $\text{RMSpE} = \sqrt{\sum_1^N \left(\frac{y_{pred,i} - y_{exp,i}}{y_{exp,i}}\right)^2}$

[c] Includes only dataset where information about the contact angle is available.

[17]. With annular geometries Liu and Winterton [59] correlation was used instead as it was specifically developed for such geometries. This fact is noted with a number in Table 6 geometry column.

According to the previous dimensional analysis of the bubble detachment phenomenon under subcooled flow boiling, the important dimensionless groups identified are plotted in Fig. 18. The aim here, is to have a global idea about the trend and the correlation degree of the different dimensionless groups identified, and not to make a comprehensive review of this effects, since this task has been individually done by each of the dataset's owners. Despite the boiling number is not identified as a functional group, it is included here because of its widespread use in past correlations. The inclusion of the boiling number is justified to capture the effect of the flow velocity rather than the Reynolds number does.

Among the different groups included, the strongest dependencies have been observed with the density ratio (Fig. 18-top-left), Prandtl number for the saturated state (Fig. 18-middle-up-left) and the Reynolds number based on flow channel dimensions (Fig. 18-top-right).

4.6. Review of the performance of previously published models

Probably due to the short range of experimental data used in deriving certain correlations, the big problem of the limited data becomes clear. A poorly conditioned dataset can result in a very biased correlation. On the one side, if only a few experimental points are available, could not reveal any important hidden dependence. On the other, a short range covered could yield to an ill conditioning of the different coefficients of the correlation.

In ~~the~~ Table 8 is shown the benchmark between some of the well-documented models for the mean bubble size found in the literature. In order to check how the different models catch the trend, the graphical output for the mean bubble diameter and the selected correlations is shown in Fig. 19. The error lines in the charts represent the ±50% deviation interval. In the evaluation, datasets without stating a value for the angle of contact have been omitted for the models and correlations requiring it.

The best two performances among all the models analyzed are the Prodanovic et al. [10] and the Brooks and Hibiki [13] proposals for flow boiling. The strategy is similar on both although Brooks and Hibiki get a plausible better error, since they considered a different scale coefficient between mini and conventional channels and they also included the Prandtl number in their correlation. Moreover, Brooks and Hibiki proposal is dated more than ten years later, so that the used sample is wider and reliable.

4.7. Proposed correlation for bubble diameter

In our proposal for the mean bubble size correlation, the capillarity length is the characteristic length selected. The new correlation includes the clearly observed dependence of the bubble size with the density ratio (pressure), the Prandtl number (thermal diffusivity) and the Reynolds number (bulk velocity). The subcooling and the superheating effect with great impact in the characteristic heats, have also been included by means of the respective Jakob numbers. Since the density ratio has been considered alone as a functional group, the numbers are presented in their simplified form (i.e. without including the densities of the fluid phases).

To catch some of the influence that the channel size has on the size of the bubbles, some authors changed the characteristic length [60] or the global scale parameter [13], to improve the correlation output. In this work, we noticed a correlation between the best scale coefficient and the hydraulic diameter of the channel. Therefore, an additional term comprising the hydraulic diameter to bubble diameter ratio has been included. Despite of the addition of the term, further work is needed to derive a complete law for characterize this effect.

The proposed correlation for the mean bubble diameter is shown in Eq. (22). The graphical output for this second presented correlation is shown in Fig. 20.

$$D_b^+ = 0.178 \cdot \rho^{*-0.676} \cdot Pr_{sat}^{0.9} \cdot Ja_W^{0.145} \cdot Ja_{sub}^{0.3} \cdot Re_{hyd}^{-0.334} \cdot \left(\frac{l_c}{D_{hyd}}\right)^{0.235} \quad (22)$$

The new proposed expression improves the previous best correlation found in the literature nearly 7% in RMSpE and more than 4% in MApE, so that the final indexes are about 36.8% and 28.9%, respectively. All these error indexes are also presented in the benchmarking (Table 8).

5. Conclusion

In this work is addressed a study about the bubble distribution in flow boiling systems. The knowledge of the shape of the diameter distribution or even the best model for describing that pdf is crucial to develop accurate calculation algorithms or develop reliable mechanistic models meant to be used is CFD solvers. In the first part of this work, the distribution model, and the variance of the diameter distributions for several experimental conditions have been studied, to develop a correlation for the width of the distributions, given as a first result. The variance of the normalized diameter distributions has found to be mainly a function of the bubble mean diameter, the pressure, the flow velocity, and the wall superheating. Also, the use of three different boiling surface morphologies in the sample, allow the inclusion of a parameter concerning the bulk morphology of the heated plate. The final correlation achieves a good error index although it was only verified with the data from this work.

In the second part, once the variance of the normalized diameters distribution is predicted, the total distribution could be estimated provided a trustworthy value for the mean bubble diameter is known for the conditions of the experimental test. With this aim, a review of past models and correlations as well as a comprehensive compilation of another author's dataset have been done. The own authors' dataset comprising almost one million of bubbles, and presented as an electronic annex, has also been included. All this data was statistically treated to get a new correlation covering a wide range of experimental conditions and facilities.

Further work is needed to improve the response and the extension of the correlation for the width of the distribution to new morphologies and surfaces. Scarce statistically significant data concerning the shape of distributions can be found in the literature, so additional data employing other fluids and surfaces are needed to improve the characterization. Moreover, further study should be developed to clarify the influence of the roughness and the surface finishing on the introduced empiric

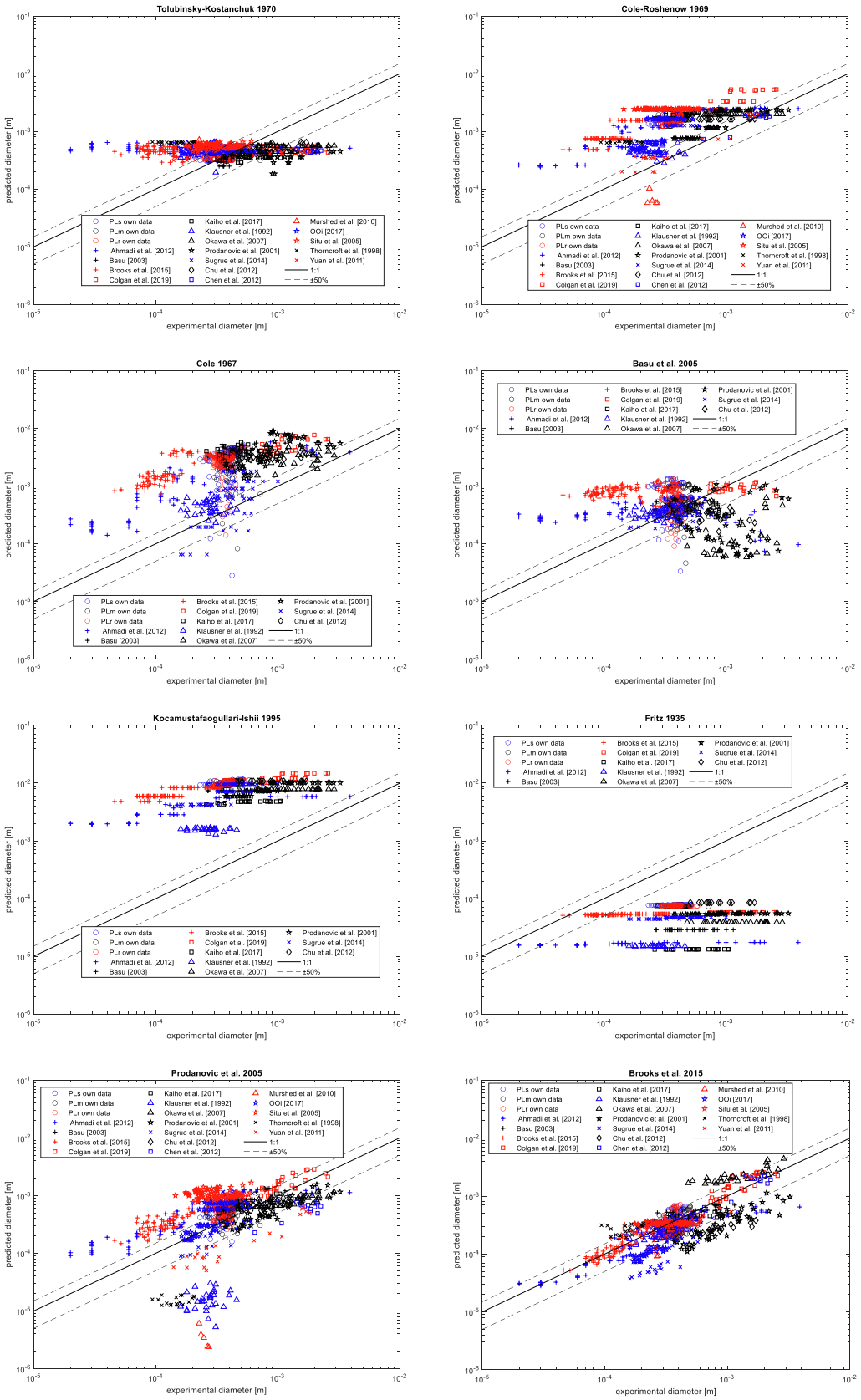

Fig. 19. Output of selected models for the whole dataset included.

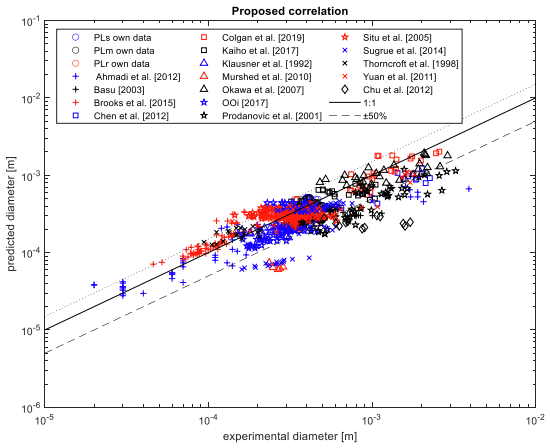

Fig. 20. Model output for the proposed correlation and selected dataset.

constant, by means of the contact angle distribution and other important wall parameters.

Also, despite noticing a trend of the bubble parameter as a function of the channel dimensions, the so limited data made impossible the proper characterization of this effect. Nowadays, the intensively use of power-electronic systems, with the employment of a big variety of shapes and enhanced heating releasing methods, justify further investigation on this topic.

CRediT authorship contribution statement

Marcos Conde-Fontenla: Conceptualization, Methodology, Formal analysis, Data curation, Visualization, Writing - original draft, Writing - review & editing. **Concepción Paz:** Conceptualization, Methodology, Supervision, Writing - review & editing, Project administration, Funding acquisition. **Miguel Concheiro:** Investigation, Validation, Data curation. **Gherhardt Ribatski:** Supervision, Visualization, Writing - review & editing.

Declaration of Competing Interest

None declared.

Acknowledgements

The authors are grateful for the financial support from the Spanish Ministry of Science and Innovation through the RTC2019-006955-4 project.

References

[1] W. Fritz, Maximum volume of vapour bubbles, Physik Zeitschr 36 (1935) 379–384.
[2] N. Zuber, Hydrodynamic Aspects of Boiling heat transfer, PhD Thesis, University of California, 1959.
[3] C.-Y. Han, P. Griffith, The mechanism of heat transfer in nucleate pool boiling, Massachusetts Institute of Technology. Division of Sponsored Research, 19, 1962.
[4] R. Cole, Bubble frequencies and departure volumes at subatmospheric pressures, AIChE J. 13 (1967) 779–783.
[5] R. Cole, W.R. Rohsenow, Correlation of bubble departure diameters for boiling of saturated liquids, Chem. Eng. Prog. Symp. 92 (1969) 211–213.
[6] V. I. Tolubinsky, D. M. Kostanchuk, Vapor bubbles growth rate and heat transfer intensity at subcooled water boiling, in Heat transfer 1970, Preprints of papers presented at the Fourth International Heat Transfer Conference, 1970, vol. 5, p. Paper No B2.8.
[7] H.C. Unal, Maximum bubble diameter, maximum bubble-growth time and bubble-growth rate during the subcooled nucleate flow boiling of water up to 17.7 MN/m2, Int. J. Heat Mass Transf. 19 (1976) 643–649.
[8] G. Kocamustafaogullari, Pressure dependence of bubble departure diameter for water, Int. Commun. Heat Mass Transfer 10 (6) (1983) 501–509.
[9] D. Farajisarir, Growth and collapse of vapour bubbles in convective subcooled boiling of water, MASc Thesis, University of British Columbia, 1993.
[10] V. Prodanovic, D. Fraser, M. Salcudean, Bubble behavior in subcooled flow boiling of water at low pressures and low flow rates, Int. J. Multiph. Flow 28 (1) (2002) 1–19.
[11] N. Basu, G.R. Warrier, V.K. Dhir, Wall heat flux partitioning during subcooled flow boiling: Part I Model development, J. Heat Transfer 127 (2) (2005) 131–140.
[12] N. Basu, "Modeling and experiments for wall heat flux partitioning during subcooled flow boiling of water at low pressures," University of California, Los Angeles, Ann Arbor, 2003.
[13] C.S. Brooks, T. Hibiki, Wall nucleation modeling in subcooled boiling flow, Int. J. Heat Mass Transf. 86 (2015) 183–196.
[14] M. C. Paz, M. Conde, E. Suárez, and M. Concheiro, "On the effect of surface roughness and material on the subcooled flow boiling of water: Experimental study and global correlation," Exp. Therm. Fluid Sci., vol. 64, pp. 114–124, 2015.
[15] C. Paz, M. Conde, J. Porteiro, M. Concheiro, Effect of heating surface morphology on the size of bubbles during the subcooled flow boiling of water at low pressure, Int. J. Heat Mass Transf. 89 (2015) 770–782.
[16] C. Paz, M. Conde, J. Porteiro, M. Concheiro, On the Application of Image Processing Methods for Bubble Recognition to the Study of Subcooled Flow Boiling of Water in Rectangular Channels, Sensors 17 (6) (Jun. 2017) 1448.
[17] M.C. Paz, M. Conde, E. Suarez, M. Concheiro, On the effect of surface roughness and material on the subcooled flow boiling of water: Experimental study and global correlation, Exp. Therm Fluid Sci. 64 (2015) 114–124.
[18] J.F. Klausner, R. Mei, D.M. Bernhard, L.Z. Zeng, Vapor bubble departure in forced convection boiling, Int. J. Heat Mass Transfer 36 (3) (1993) 651–662.
[19] N. Colgan, J.L. Bottini, Z.J. Ooi, C.S. Brooks, Experimental study of wall nucleation characteristics in flow boiling under subatmospheric pressures in a vertical square channel, Int. J. Heat Mass Transf. 134 (May 2019) 58–68.
[20] Z.J. Ooi, V. Kumar, J.L. Bottini, C.S. Brooks, Experimental investigation of variability in bubble departure characteristics between nucleation sites in subcooled boiling flow, Int. J. Heat Mass Transf. 118 (Mar. 2018) 327–339.
[21] R. Martınez-Cuenca, C.S. Brooks, J.E. Juliá, T. Hibiki, M. Ishii, Stochastic Nature of Wall Nucleation and Its Impact on the Time Average Boundary Condition, J. Heat Transfer 137 (2) (Feb. 2015).
[22] K. Kaiho, T. Okawa, K. Enoki, Measurement of the maximum bubble size distribution in water subcooled flow boiling at low pressure, Int. J. Heat Mass Transf. 108 (May 2017) 2365–2380.
[23] Koichi Takagi, Shinji Kumagai, Ichiro Matsunaga, Yukinori Kusaka, Application of inverse Gaussian distribution to occupational exposure data, Ann. Occup. Hygiene 41 (5) (Oct. 1997) 505–514.
[24] S. Pasari, Inverse Gaussian versus lognormal distribution in earthquake forecasting: keys and clues, J. Seismolog. 23 (3) (Mar. 2019) 537–559.
[25] J. L. Folks, R. S. Chhikara, The Inverse Gaussian Distribution and Its Statistical Application–A Review. Series B (Methodological), Vol. 40, No. 3 (1978), pp. 263-289 Published by: Wiley for the Royal Statistical Society Stable URL: https://www.jstor.org/stable/2984691 Accessed: 03-10-2019 17:53 UTC," Journal of the Royal Statistical Society, 2019.
[26] E.L. Crow, K. Shimizu, Lognormal distributions: theory and applications, Taylor & Francis Inc, 1987.
[27] S. Kandlikar and B. Stumm, "A Control Volume Approach for Investigating Forces on a Departing Bubble Under Subcooled Flow Boiling," Journal of Heat Transfer-transactions of The Asme - J HEAT TRANSFER, vol. 117, 1995.
[28] R. Maurus, T. Sattelmayer, Bubble and boundary layer behaviour in subcooled flow boiling, Int. J. Therm. Sci. 45 (3) (2006) 257–268.
[29] R. Maurus, V. Ilchenko, T. Sattelmayer, Study of the bubble characteristics and the local void fraction in subcooled flow boiling using digital imaging and analysing techniques, Exp. Therm Fluid Sci. 26 (2–4) (2002) 147–155.
[30] J.P. McHale, S.V. Garimella, Nucleate boiling from smooth and rough surfaces - Part 2: Analysis of surface roughness effects on nucleate boiling, Exp. Therm Fluid Sci. 44 (2013) 439–455.
[31] C. Paz, M. Conde, J. Porteiro, M. Concheiro, Effect of heating surface morphology on active site density in subcooled flow nucleated boiling, Exp. Therm Fluid Sci. 82 (Apr. 2017) 147–159.
[32] Geometrical product specifications (GPS) — Surface texture: Areal — Part 2: Terms, definitions and surface texture parameters. International Organization for Standardization, 2012.
[33] R.L.Z. Klausner, J.F. Bernhard, D.M. Mei Zeng, A unified model for the prediction of bubble detachment diameters in boiling systems-II. Flow boiling, Int. J. Heat Mass Transfer 36 (9) (1993) 2271–2279.
[34] G.H. Yeoh, J.Y. Tu, A unified model considering force balances for departing vapour bubbles and population balance in subcooled boiling flow, Nucl. Eng. Des. 235 (10–12) (May 2005) 1251–1265.
[35] H. Steiner, A. Kobor, L. Gebhard, A wall heat transfer model for subcooled boiling flow, Int. J. Heat Mass Transf. 48 (19–20) (2005) 4161–4173.
[36] Y.-J. Cho, S.-B. Yum, J.-H. Lee, G.-C. Park, Development of bubble departure and lift-off diameter models in low heat flux and low flow velocity conditions, Int. J. Heat Mass Transf. 54 (15–16) (Jul. 2011) 3234–3244.
[37] R. Sugrue, J. Buongiorno, A modified force-balance model for prediction of bubble departure diameter in subcooled flow boiling, Nucl. Eng. Des. 305 (Aug. 2016) 717–722.
[38] J. Yoo, C.E. Estrada-Perez, Y.A. Hassan, Area of bubble influence due to sliding bubbles in subcooled boiling flow, Int. J. Heat Mass Transf. 125 (Oct. 2018) 43–52.
[39] T. Mazzocco, W. Ambrosini, R. Kommajosyula, E. Baglietto, A reassessed model for mechanistic prediction of bubble departure and lift off diameters, Int. J. Heat Mass Transf. 117 (Feb. 2018) 119–124.

[40] J.S. Kim, Y.-N. Kim, H.K. Cho, Predicting the sliding bubble velocity on the lower part of a horizontal tube heater under natural convection based on force balance analysis, Int. J. Heat Mass Transf. 151 (Apr. 2020) 119453.
[41] B.B. Mikic, W.M. Rohsenow, A New Correlation of Pool-Boiling Data Including the Effect of Heating Surface Characteristics, J. Heat Transfer 91 (2) (May 1969) 245–250.
[42] N. Kurul, M.Z. Podowski, On the modeling of multidimensional effects in boiling channels. Proceedings of the 27th National Heat Transfer Conference, Minneapolis, Minn, USA, 1991.
[43] G.R. Warrier, V.K. Dhir, Heat Transfer and Wall Heat Flux Partitioning During Subcooled Flow Nucleate Boiling—A Review, J. Heat Transfer 128 (12) (2006) 1243–1256.
[44] N. Basu, G.R. Warrier, V.K. Dhir, Onset of nucleate boiling and active nucleation site density during subcooled flow boiling, J. Heat Transfer 124 (4) (2002) 717–728.
[45] R. Mei, J.F. Klausner, G.E. Thorncroft, An experimental investigation of bubble growth and detachment in vertical upflow and downflow boiling, Int. J. Heat Mass Transfer 41 (23) (Dec. 1998) 3857–3871.
[46] R. Situ, T. Hibiki, M. Ishii, M. Mori, Bubble lift-off size in forced convective subcooled boiling flow, Int. J. Heat Mass Transf. 48 (25–26) (Dec. 2005) 5536–5548.
[47] T. Okawa, H. Kubota, T. Ishida, Simultaneous measurement of void fraction and fundamental bubble parameters in subcooled flow boiling, Nucl. Eng. Des. 237 (10) (May 2007) 1016–1024.
[48] S.M.S. Murshed, K. Vereen, D. Strayer, R. Kumar, An experimental investigation of bubble nucleation of a refrigerant in pressurized boiling flows, Energy 35 (12) (Dec. 2010) 5143–5150.
[49] D. Yuan, L. Pan, D. Chen, H. Zhang, J. Wei, Y. Huang, Bubble behavior of high subcooling flow boiling at different system pressure in vertical narrow channel, Appl. Therm. Eng. 31 (16) (Nov. 2011) 3512–3520.
[50] I.C. Chu, H.C. No, C.-H. Song, Bubble Lift-off Diameter and Nucleation Frequency in Vertical Subcooled Boiling Flow, J. Nucl. Sci. Technol. 48 (6) (Jun. 2011) 936–949.
[51] D. Chen, L. Pan, S. Ren, Prediction of bubble detachment diameter in flow boiling based on force analysis, Nucl. Eng. Des. 243 (Feb. 2012) 263–271.
[52] R. Ahmadi, T. Ueno, T. Okawa, Bubble dynamics at boiling incipience in subcooled upward flow boiling, Int. J. Heat Mass Transf. 55 (1–3) (Jan. 2012) 488–497.
[53] R. Sugrue, J. Buongiorno, T. McKrell, An experimental study of bubble departure diameter in subcooled flow boiling including the effects of orientation angle, subcooling, mass flux, heat flux, and pressure, Nucl. Eng. Des. 279 (Nov. 2014) 182–188.
[54] C.S. Brooks, N. Silin, T. Hibiki, M. Ishii, Experimental Investigation of Wall Nucleation Characteristics in Flow Boiling, J. Heat Transfer 137 (5) (May 2015) 51501.
[55] C.S. Brooks, B. Ozar, T. Hibiki, M. Ishii, Interfacial area transport of subcooled boiling flow in a vertical annulus, Nucl. Eng. Des. 268 (Mar. 2014) 152–163.
[56] Z.J. Ooi, Experimental investigation of variability between nucleation sites in flow boiling, Graduate College of the University of Illinois at Urbana-Champaign, Urbana, IL-USA, 2017.
[57] J.C. Chen, Correlation for boiling heat transfer to saturated fluids in convective Flow, Ind. Eng. Chem. Process Des. Dev. 5 (3) (1966) 322–329.
[58] D. Butterworth, The correlation of cross flow pressure drop data by means of a permeability concept, UKAEA Report AERE-R9435 (1979).
[59] Z. Liu, R.H.S. Winterton, A general correlation for saturated and subcooled flow boiling in tubes and annuli, based on a nucleate pool boiling equation, Int. J. Heat Mass Transf. 34 (11) (1991) 2759–2766.
[60] M.M. Shah, Comprehensive correlations for heat transfer during condensation in conventional and mini/micro channels in all orientations, Int. J. Refrig 67 (Jul. 2016) 22–41.